Supporting Information

Arakel et al. 10.1073/pnas.1603544113

SI Methods

Yeast Strains. The δc* strain was created using a *HIS3*-containing plasmid (pRS303) carrying *ARCN1* that was integrated into the genome and selected on 5-FOA for the loss of the *ret2-1* carrying *URA3* plasmid. TAP-tagged β′-COP (*SEC27*) strains were created by amplifying the C-terminal TAP::*URA3* cassette from the yeast TAP-tagged collection (Open Biosystems). The cassette was inserted by homologous recombination into the respective strains and verified by PCR using ORF-specific primers from genomic DNA. Yeast strains and plasmids used in this study have been listed in Tables S1 and S2, respectively.

Secretion Assay. Stationary phase cultures grown in minimal media were diluted into complete/rich medium (YPAD; OD_{600} of 0.5) and grown to midlogarithmic phase (~2 h). The cells were harvested, washed, and resuspended in fresh medium at equivalent densities (OD_{600} of 0.5). Following a further 2 h of growth, 1.5 mL of the culture was centrifuged at 13,000 × *g* (1 min) and 1.35 mL of the supernatant/growth medium was collected. Proteins in the extracellular media were precipitated by the addition of trichloroacetic acid [16% (vol/vol)] (TCA) and incubated on ice for 15 min. The proteins were harvested by centrifugation at 15,000 × *g* at 4 °C for 15 min, acetone-washed twice, and air-dried at room temperature and resuspended in 35 μL of SDS/PAGE 1× SDS sample buffer supplemented with 1 mM DTT and 50 mM Tris, pH 8.8. The harvested cell pellets were resuspended in 100 mM NaOH for 10 min and subsequently centrifuged at 13,000 × *g* before lysis in SDS/PAGE sample buffer. The cell densities were determined (OD_{600}) and equivalent amounts analyzed by SDS/PAGE and Western blotting. Accordingly, normalized volumes (depending on the cell densities) of the precipitated medium were analyzed. The blots were scanned and quantified using an Odyssey Sa Infrared imaging system (IRDye LiCOR secondary antibody).

Fluorescence Microscopy. Manual microscopy was performed using a Delta Vision RT (Applied Precision) microscope using an oil immersion 100×/0.35-1.5 Uplan Apo objective and specific band pass filter sets for YFP. Images were captured using a Coolsnap HQ (Photometrics) camera. All images shown are representative of several independent experiments. Automated microscopy was performed using an Imaging Machine 03-dual (Acquifer) widefield high-content screening microscope, equipped with a white light-emitting diode (LED) array for bright-field imaging, an LED fluorescence excitation light source, an sCMOS (2,048 × 2,048 pixel) camera, and a stationary plate holder in combination with movable optics. Images were acquired in bright field and with 470-nm filter cubes (Ex 469/35, Em 525/39, dichroic 497) using three z-slices (dz of 1 μm) and a 40× CFI Super Plan Fluor ELWD N.A. 0.60 (Nikon). The focal plane was detected in the bright-field channel using a yeast autofocus algorithm.

Purification of GST Fusion Proteins. Rosetta (DE3) and BL21 (pREP4) *Eschericia coli* strains containing the GST fusion constructs were induced by the addition of 0.2 mM isopropyl β-D-1-thiogalactopyranoside at OD_{600} 0.8 for 3 h at 30 °C or for 16 h at 18 °C. Cells were harvested and sonicated in lysis buffer [20 mM Hepes, pH 6.8, 2% (vol/vol) glycerol, 150 mM KAc, 5 mM $Mg(Ac)_2$, 1 mM EDTA, 1 mM DTT, and 1 mM PMSF]. Lysates were cleared first at 5,000 × *g* for 5 min and subsequently at 100,000 × *g* for 30 min. The GST-fusion proteins/baits were purified by incubating lysates with GSH-Sepharose. The affinity matrix was washed five times with lysis buffer and eluted with elution buffer [20 mM Hepes, pH 9.5, 10 mM glutathione (GSH), 5% (vol/vol) glycerol, 150 mM KAc, 5 mM $Mg(Ac)_2$, 1 mM EDTA, and 1 mM DTT]. The baits were dialyzed overnight in dialysis buffer (200 mM NaCl, 20 mM Hepes, pH 7.4, and 1 mM DTT) before use in binding assays.

Purification of Yeast Coatomer. Yeast cells were grown to early stationary phase and harvested at 5,000 × *g* for 10 min. A cell pellet corresponding to ~5 mL (packed volume) was flash-frozen in liquid nitrogen, crushed by hand, resuspended in lysis buffer [10 mM sodium phosphate, pH 7.4, 150 mM NaCl, 1 mM EDTA, 1.5 mM benzamidine, 1 mM PMSF/APMSF, complete protease inhibitor tablet (Roche), and 5 μg/mL leupeptin/pepstatin] and subsequently dounce-homogenized (25 strokes). The lysate was supplemented with 1% Triton X-100 and incubated on ice for 30 min and centrifuged first at 5,000 × *g* at 4 °C for 10 min and at 100,000 × *g* at 4 °C for 30 min. Following ultracentrifugation the extracts were passed through a 0.45-μm filter and diluted fivefold in lysis buffer. IgG Sepharose was incubated with the supernatant for 30 min at 4 °C and packed/sedimented in a column. The affinity matrix was washed four times with lysis buffer (supplemented with 0.1% Triton X-100) and once with tobacco etch virus (TEV) cleavage buffer (10 mM Tris·HCl, pH 8.0, 150 mM NaCl, 0.1% Triton X-100, 0.5 mM EDTA, and 1 mM DTT). Coatomer was eluted by TEV cleavage for 1 h at 16 °C. The eluted coatomer was used for binding assays.

Binding Assays. Purified bait (7.5 μg) was immobilized on 20 μL GSH-Sepharose and incubated with purified coatomer or cytosol for between 1–2 h at 4 °C. The matrix was subsequently washed four times with binding buffer [20 mM Hepes, pH 7.4, 2% (vol/vol) glycerol, 150 mM KAc, 5 mM $Mg(Ac)_2$, 1 mM EDTA, 1 mM DTT, and 0.1% Triton X-100] and eluted with 1x SDS sample buffer containing 1mM DTT, resolved by SDS/PAGE, transferred onto nitrocellulose membranes by Western blotting, and detected with the indicated antibodies. The blots were scanned and quantified using an Odyssey Sa Infrared imaging system (IRDye LiCOR secondary antibody).

Miscellaneous. Secondary protein structure prediction from amino acid sequence was performed on the Jpred server (http://www.compbio.dundee.ac.uk/jpred/) (39). Structures were rendered from the indicated PDB coordinates using the PyMOL Molecular Graphics System, Version 1.7.4.4 (Schrödinger, LLC). Phosphorylation prediction from amino acid sequence was performed on the NetPhos 2.0 Server (http://www.cbs.dtu.dk/services/NetPhos/) (35) and the NetPhosYeast 1.0 Server (http://www.cbs.dtu.dk/services/NetPhosYeast/) (36). Helical wheel projections were generated using the HeliQuest server (http://heliquest.ipmc.cnrs.fr/) (40).

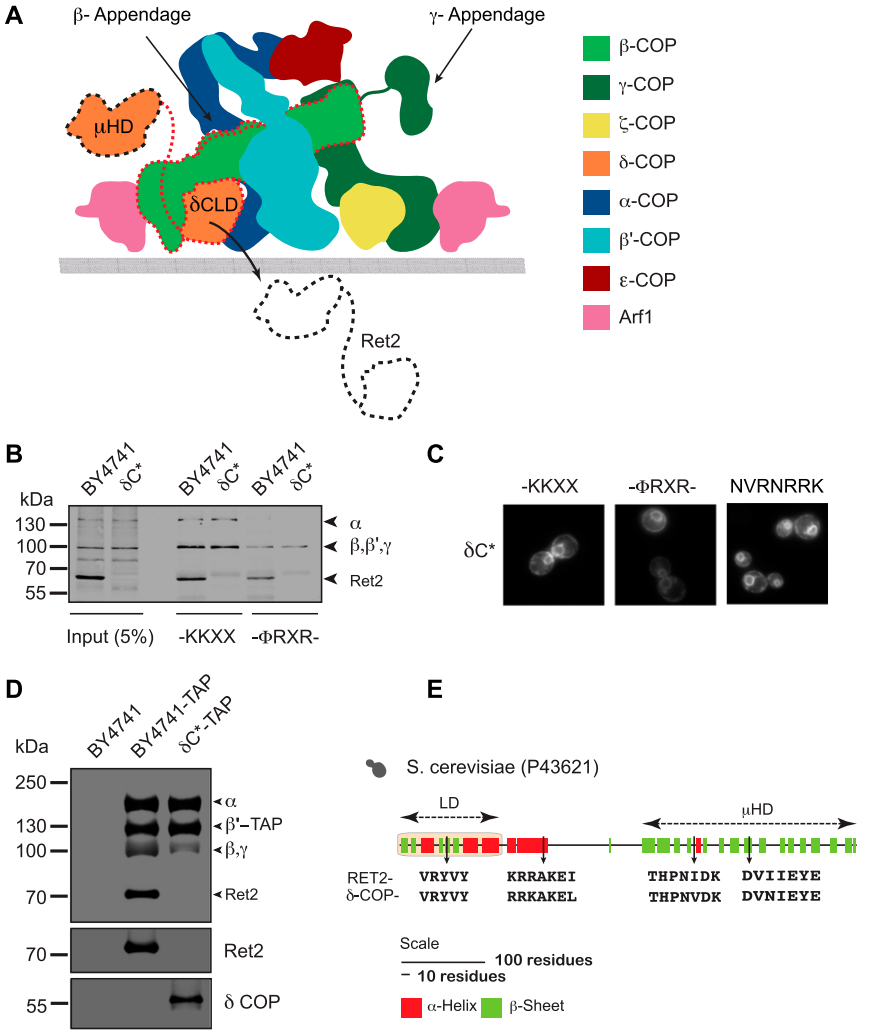

Fig. S1. The *B. taurus* δ-COP subunit *ARCN1* functionally complements the essential yeast δ-COP subunit *RET2* despite sharing only 34% sequence similarity. (*A*) Schematic illustration of membrane-associated coatomer based on ref. 3. The Ret2 subunit of the yeast COPI coat was replaced with the Archain subunit of *B. taurus* in the δc* strain. (*B*) Binding of coatomer from yeast cytosol to GST fusion proteins of the cytosolic tail of Mst27 presenting the indicated di-lysine (-KKXX) or Arg-based (-ΦRXR) ER retrieval signals (14). Cytosol was prepared from a wild-type BY4741 strain or the δc* strain. The bound fraction was eluted from the affinity matrix and analyzed by SDS/PAGE followed by immunoblot analysis using an antiserum recognizing all seven coatomer subunits. Five percent of the input cytosol was loaded as a control. (*C*) Localization analysis of a Pmp2YFP reporter protein presenting a di-lysine (-KKXX), an Arg-based (-ΦRXR), or a weak (NVRNRRK) Arg-based ER retrieval signal (14) in the δC* strain. (*D*) TAP purification of coatomer from a Sec27-TAP (β′-COP) tagged wild-type BY4741 or δc* strain. The eluted coat was analyzed by SDS/PAGE followed by immunoblot analysis using an antiserum recognizing all seven coatomer subunits and antibodies specific for Ret2 and δ-COP. Note that the signal intensity of the trunk/ F-sub complex (β, γ) in the δc* strain is significantly lower than that of the wild-type BY4741 strain, presumably owing to the dissociation of the trunk during purification. The signal intensity of the cage/ B-subcomplex is identical in both BY4741 and δc* strains. (*E*) The boundaries at which the chimaeras were constructed, mapped onto the predicted secondary structure of Ret2. The longin domain (LD) and the μHD are indicated.

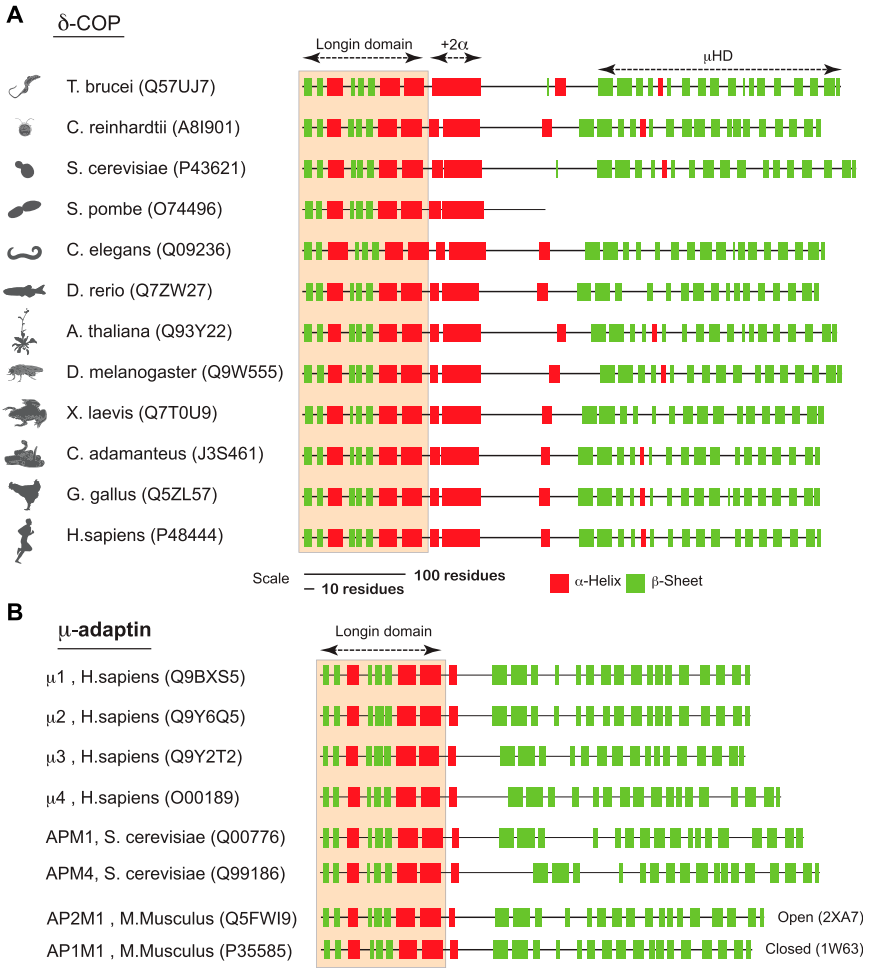

Fig. S2. Prediction-based structural alignment of δ-COP and μ-adaptin reveals minor but important variations in its architecture. (*A*) Schematic representation of JPred secondary structure predictions of the δ-COP subunit from different species. The longin domain, the two adjoining helices (+2α), and the μHD are conserved from simple eukaryotes such as yeast to higher eukaryotes such as mammals. Note that *S. pombe* lacks a functional μHD. The UniProt accession numbers have been provided in parentheses. (*B*) Schematic representation of JPred secondary structure predictions of the μ-adaptin subunits from different species. The JPred secondary structure predictions indicate significant structural similarity between the μ-adaptin and the δ-COP subunit (*A*), apart from the second helix C-terminal to the longin domain. The UniProt accession numbers have been provided in parentheses.

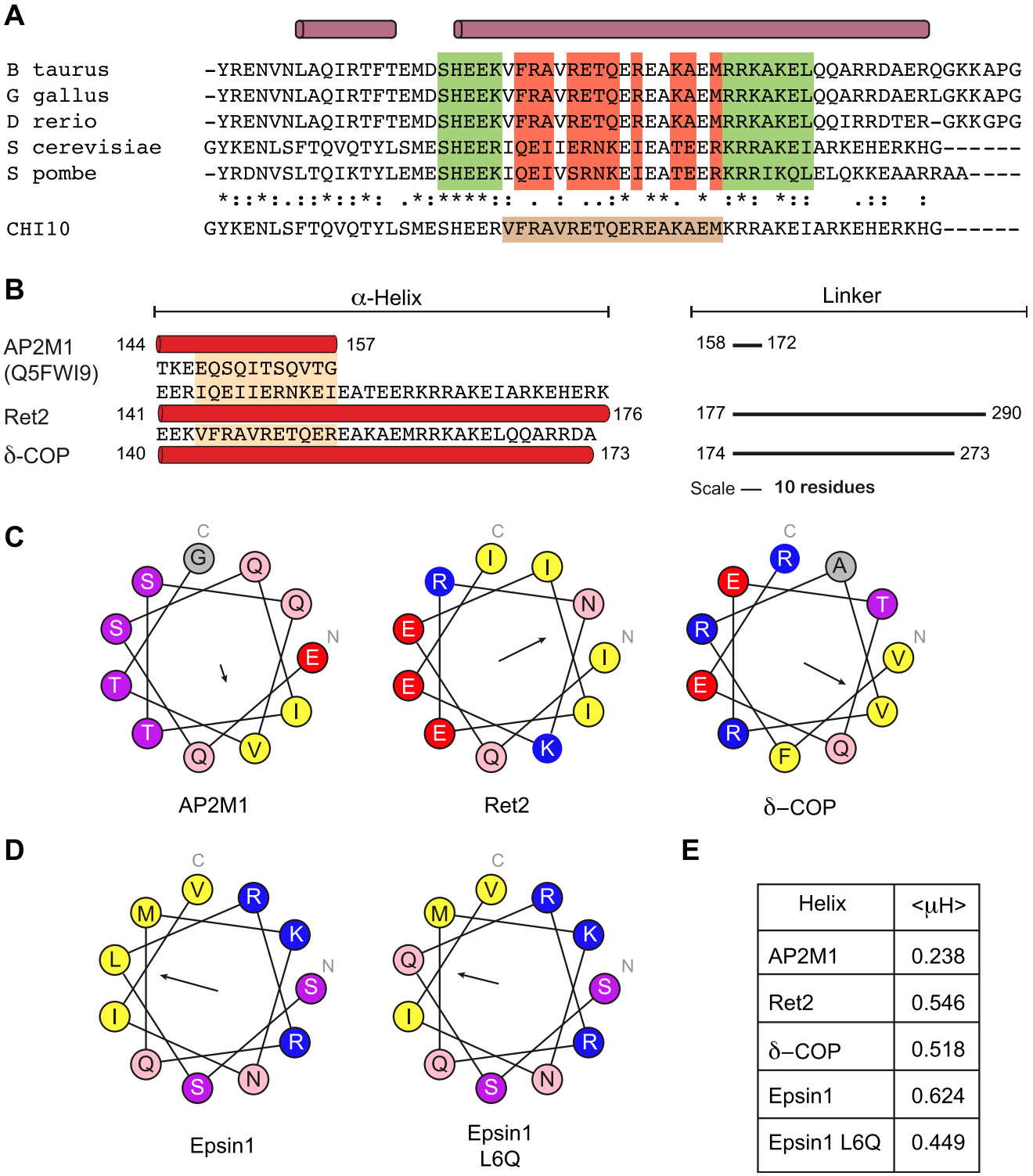

Helix	<μH>
AP2M1	0.238
Ret2	0.546
δ–COP	0.518
Epsin1	0.624
Epsin1 L6Q	0.449

Fig. S3. The identified helix has characteristics of an amphipathic helix. (*A*) Sequence alignment of the two predicted helices C-terminal to the δ-COP longin domain from different species. The highly conserved regions of the second helix have been highlighted in green. Chimaera 10 (CHI10) was created by replacing the 17 residues within the conserved regions of Ret2 with the corresponding residues of *B. taurus* Archain. Unconserved residues in this minimal region have been highlighted in red. (*B*) Amino acid sequence and length of the critical helix of μ-adaptin, Ret2, and δ-COP (*Left*). The residue positions are indicated. Schematic representation of the linker lengths connecting the critical helix and the μHD in μ-adaptin, Ret2 and δ-COP (*Right*). (*C*) Helical wheel representation of the helices of μ-adaptin, Ret2, and δ-COP. Residues have been color-coded: yellow for hydrophobic, purple for serine and threonine, blue for basic, red for acidic, pink for asparagine and glutamine, and gray for alanine and glycine. The helical wheel corresponds to the region highlighted in orange in *B*. The arrow in the helical wheel corresponds to the hydrophobic moment and its length reflects the size of the hydrophobic moment. (*D*) Helical wheel representation of the α_0 helix of Epsin and mutant (L6Q) after ref. 37. The residues are color-coded as in *C*. (*E*) Table summarizing the hydrophobic moment (<μH>) obtained from helical wheel analysis using HeliQuest (40).

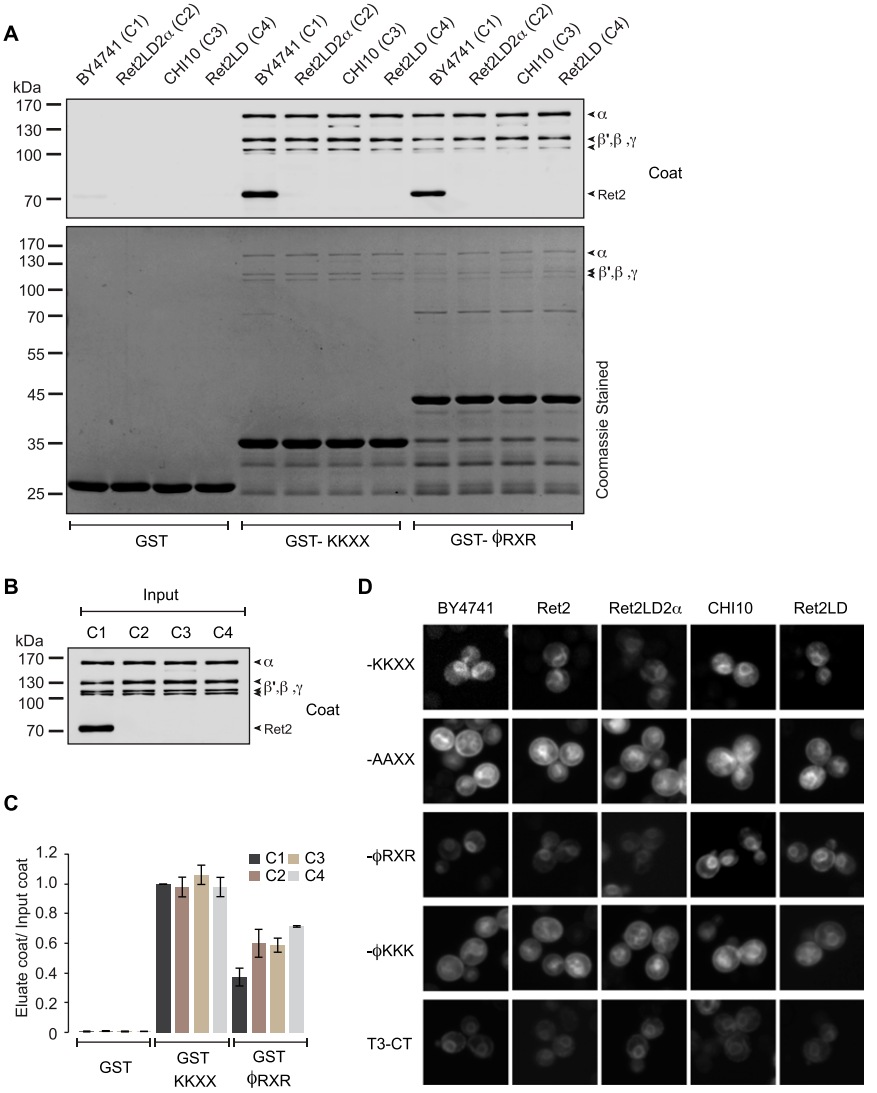

Fig. S4. Mutations in the identified helix do not impinge on the canonical retrieval functions of other COPI subunits. (*A*) Binding of TAP-purified coatomer to GST fusion proteins of the cytosolic tail of Mst27 presenting the indicated di-lysine (-KKXX) or Arg-based (-ΦRXR) ER retrieval signals. Coat was purified from a wild-type BY4741 (C1) strain or strains expressing a Ret2LD2α (C2), CHI10 (C3), and Ret2LD (C4) variant of coat. The bound fraction was eluted from the affinity matrix and analyzed by SDS/PAGE followed by immunoblot analysis using an antiserum recognizing all seven coatomer subunits. C2, C3, and C4 contain a truncated Ret2 subunit, lacking the μHD that the coat antiserum detects. The purified coats were loaded as an input control (*B*). (*C*) Bar graph of the relative amounts of bound COPI as quantified by the densitometric analysis of three independent immunoblots similar to that depicted in *A*. The signal intensity of eluted COPI was normalized to the signal intensity of input COPI to correct for differences in the amount of coat used in each case. Error bars depict SEM. (*D*) Localization analysis of a Pmp2YFP reporter protein presenting a di-lysine (-KKXX), an Arg-based ER retrieval signal (-ΦRXR), its inactive mutants (-AAXX and -ΦKKK, respectively), or the C-terminus of the TASK3 ion channel (T3-CT) with a COPI binding signal [-KRRKSV (26)] in a wild-type strain, or a *ret2* deletion strain expressing wild-type Ret2 or variants Ret2LD2α, CHI10, or Ret2LD.

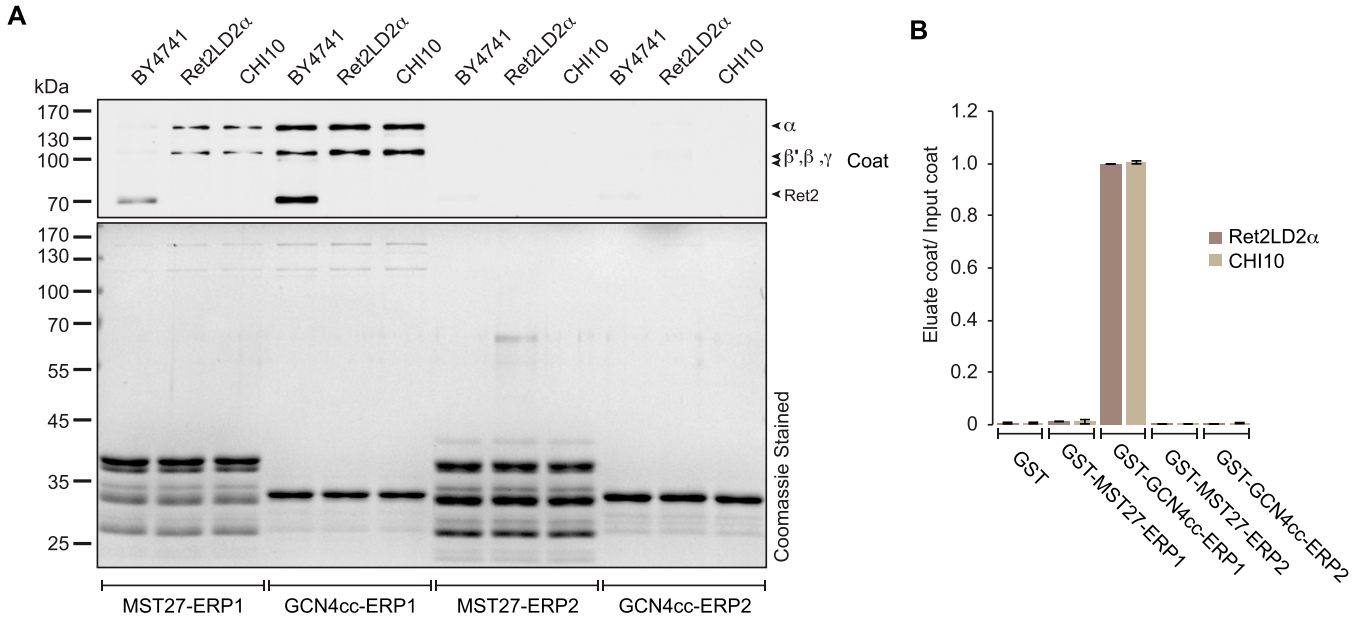

Fig. S5. Other canonical retrieval functions of COPI are unperturbed in cells with mutant coatomer, supporting a specific defect in the HDEL-based retrieval system. (*A*) Binding of TAP-purified coatomer to GST fusion proteins of the cytosolic tail of Mst27 or the Gcn4 coiled-coil forming domain presenting the di-lysine (-KXKXX) ER retrieval signals of Erp1 and a control, Erp2. Coat was purified from a wild-type BY4741 strain or strains containing a Ret2LD2α and CHI10 variant of coat. The bound fraction was eluted from the affinity matrix and analyzed by SDS/PAGE followed by immunoblot analysis using an antiserum recognizing all seven coatomer subunits. (*B*) Bar graph of the relative amounts of eluted/bound COPI as quantified by the densiometric analysis of three independent immunoblots similar to that depicted in *A*. The signal intensity of eluted COPI was normalized to the signal intensity of input COPI to correct for differences in the amount of coat used in each case. Error bars depict SEM.

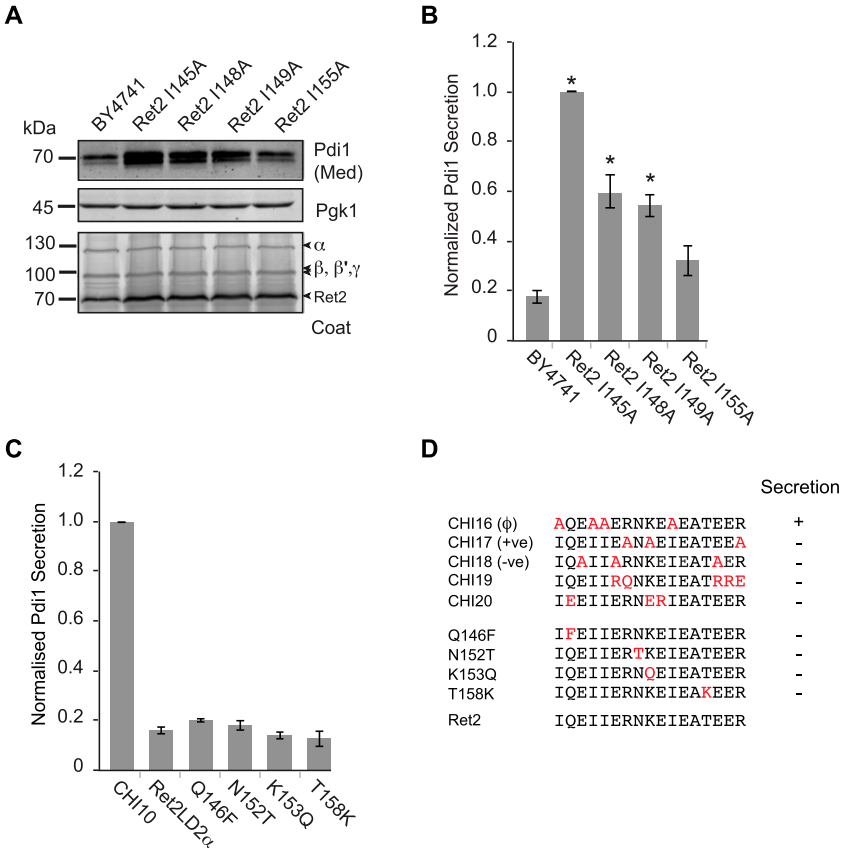

Fig. S6. Three isoleucines within the identified helix are critical for its function. (*A*) Mutation of the hydrophobic residues within the critical stretch of the second helix C-terminal to the longin domain results in the secretion of HDEL-bearing proteins. A *ret2* deletion strain was rescued with plasmids containing the indicated Ret2 variants. Proteins secreted into the culture medium (i.e., extracellular) were concentrated and harvested by TCA precipitation and analyzed by SDS/PAGE, followed by immunoblot analysis using antibodies specific for Pdi1. Cell pellets from the same cultures were also similarly analyzed using antibodies specific for Pgk1 and COPI. (*B*) Bar graph of the relative amounts of Pdi1 secreted into the culture medium as quantified by densitometric analysis of immunoblots similar to that depicted in *A*. Quantification of six independent experiments. Error bars depict SEM. (*C*) Same analysis as in *A* and *B* for constructs with individual residues within the critical helix changed from the residue present in Ret2 to that present in bovine δ-COP. Quantification of four independent experiments. Error bars depict SEM. (*D*) Qualitative summary of results obtained in *B* and *C*.

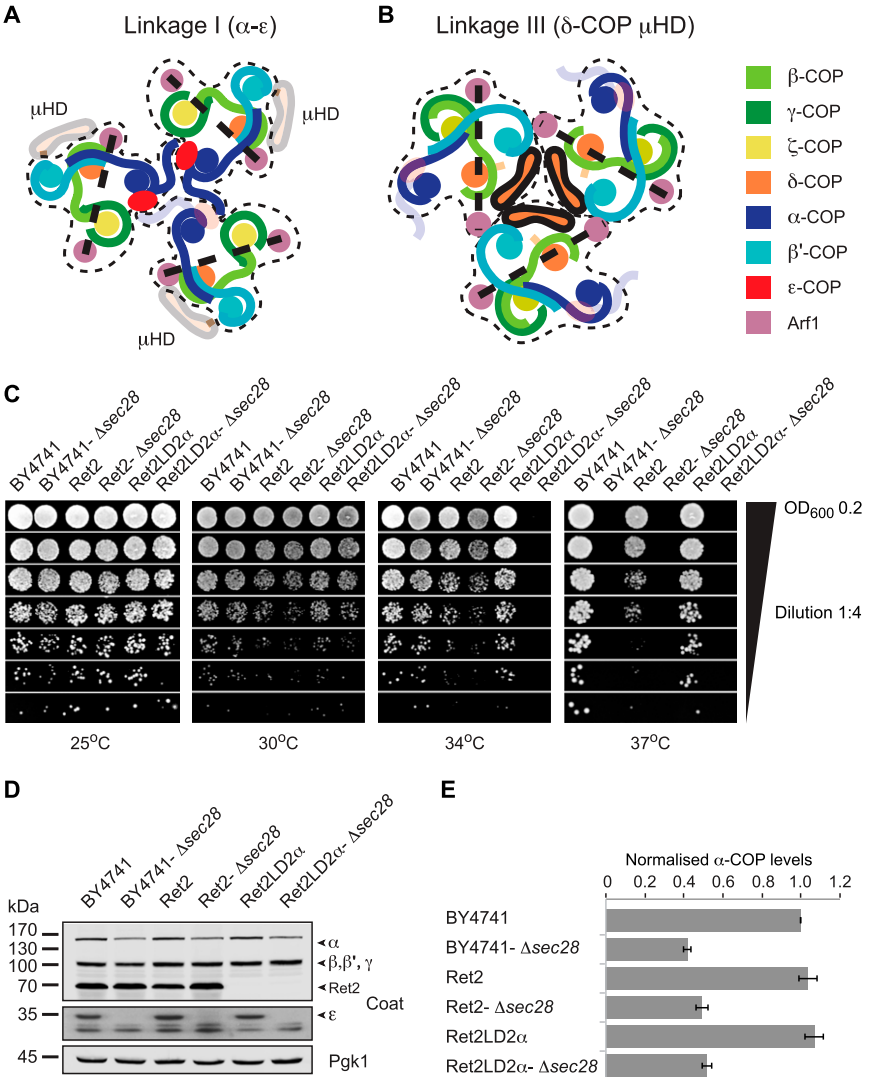

Fig. S7. Linkages mediated by the ε-COP subunit or δ-COP μHD of coatomer are nonessential. Schematic illustration of the basic building block of the COPI coat, a triad linkage of coatomers, based on the structural model proposed by Dodonova et al. (3). Coatomer triads are thought to be linked by sets of interactions involving flexible domains such as ε-COP and the C-terminal domain of α-COP (Linkage I) (*A*) or via the μHD of δ-COP (Linkage III) (*B*). Note that the δ-COP μHD is either at the periphery or at the core of the triad depending on the type of linkage. These 2D schematic representations build on the crystal structures of PDB ID codes 5A1V and 5A1X, respectively. Unresolved domains such as the μHD in linkage I and α_c and ε in linkage III are rendered translucently. (*C*) Growth assay demonstrating that the combined deletion of the Ret2 μHD and the ε-COP subunit does not affect viability up to 34 °C. The indicated yeast strains were grown to stationary phase, washed, and normalized to OD_{600} and serial dilutions were spotted onto YPAD agar and incubated at 25 °C, 30 °C, 34 °C, or 37 °C for 2 d. (*D*) SDS/PAGE and Western blot analysis of the indicated strains using antibodies specific for coat and Pgk1. (*E*) Bar graph of the relative amounts of α-COP in the indicated strains, as quantified by the densiometric analysis of three independent immunoblots similar to that depicted in *D*. Error bars depict SEM. Note that simultaneous deletion of the μHD neither suppresses nor exacerbates the lower steady-state levels of α-COP observed in the *sec28* deletion strain. This indicates that deletion of the μHD does not further destabilize the coat and excludes the hypothesis that one type of linkage may compensate for the loss of the other.

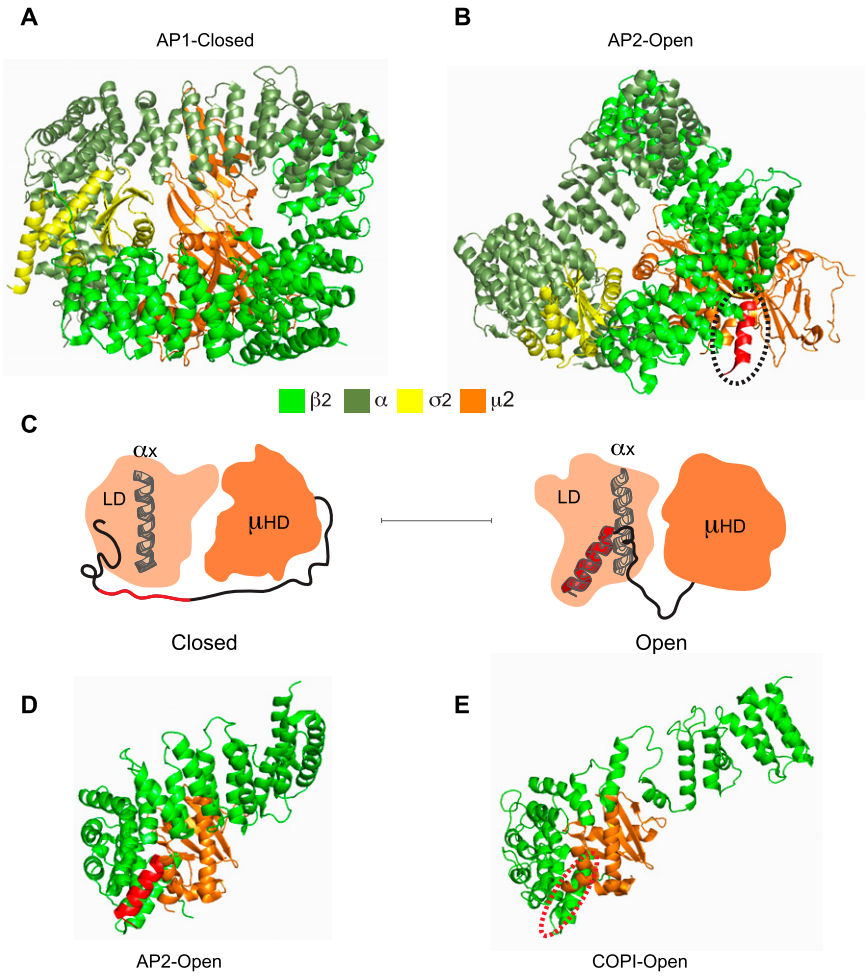

Fig. S8. By analogy to AP2, the identified region may serve as a pivot around which δ-COP is structurally reorganized upon membrane recruitment of COPI. The AP2 adaptor complex undergoes a large-scale conformational change upon membrane recruitment, transitioning from a closed form (*A*) to an open structure (*B*). This change results in the relocation of the two large adaptor subunits, the C-terminal μ-adaptin subunit (which becomes coplanar with the membrane) and the transformation of an unstructured μ-adaptin linker to a helix (colored in red), which then binds back onto the complex. This structural rearrangement exposes previously occluded cargo and lipid binding sites. *A* and *B* correspond to the crystal structure of PDB ID codes 1W63 and 2XA7 (11, 41), respectively. (*C*) Schematic representation of the structural rearrangement upon membrane association where the unstructured linker transforms into an α-helix in the open conformation. The longin domain (LD), the second α-helix of the LD (α_x), and the μHD of μ-adaptin have been highlighted for orientation. Comparison of the crystal structure of the β2-μ2-adaptin dimer (*D*) and the cryo-EM tomography derived β-δ-COP dimer (*E*). The β-δ-COP dimer appears as a "hyperopen" form compared with the β2-μ2-adaptin dimer. Note that the identified helix (corresponding to the second helix C-terminal to the longin domain) is absent in the homology model (marked with a red dotted ellipse).

Table S1. Yeast strains used in this study

No.	*S.cerevisiae* strains	Genotype	Source
1.	BY4741 (WT)	*MATa his3Δ0 leu2Δ0 met15Δ0 ura3Δ0*	Euroscarf
2.	*K60*	(*BY4743 Spore*) *MATa his3Δ1 leu2Δ0 met15Δ0 ura3Δ0; YFR051c::kanMX4; p416 ret2-1*	14
3.	δc*	(*BY4743 Spore*) *MATa his3Δ1 leu2Δ0 met15Δ0 ura3Δ0; YFR051c::kanMX4; pRS303 Btδ*COP	This study
4.	Δ*erd1*		Euroscarf
5.	Ret2	(*BY4743 Spore*) *MATa his3Δ1 leu2Δ0 met15Δ0 ura3Δ0; YFR051c::kanMX4; p415 ret2*	This study
6.	Ret2LD2α	(*BY4743 Spore*) *MATa his3Δ1 leu2Δ0 met15Δ0 ura3Δ0; YFR051c::kanMX4; p415 ret2LD2α*	This study
7.	δCLD2α	(*BY4743 Spore*) *MATa his3Δ1 leu2Δ0 met15Δ0 ura3Δ0; YFR051c::kanMX4; p415 δCLD2α*	This study
8.	Ret2LD	(*BY4743 Spore*) *MATa his3Δ1 leu2Δ0 met15Δ0 ura3Δ0; YFR051c::kanMX4; p415 ret2LD*	This study
9.	δCLD	(*BY4743 Spore*) *MATa his3Δ1 leu2Δ0 met15Δ0 ura3Δ0; YFR051c::kanMX4; p415 δCLD*	This study
10.	Ret2LD+δC2α	(*BY4743 Spore*) *MATa his3Δ1 leu2Δ0 met15Δ0 ura3Δ0; YFR051c::kanMX4; p415 ret2LD$_{+\delta C2\alpha}$*	This study
11.	δCLD+Ret2 2α	(*BY4743 Spore*) *MATa his3Δ1 leu2Δ0 met15Δ0 ura3Δ0; YFR051c::kanMX4; p415 δCLD$_{+Ret2\ 2\alpha}$*	This study
12.	CHI 9	(*BY4743 Spore*) *MATa his3Δ1 leu2Δ0 met15Δ0 ura3Δ0; YFR051c::kanMX4; p415 CHI-9*	This study
13.	CHI 10	(*BY4743 Spore*) *MATa his3Δ1 leu2Δ0 met15Δ0 ura3Δ0; YFR051c::kanMX4; p415 CHI-10*	This study
14.	CHI 12	(*BY4743 Spore*) *MATa his3Δ1 leu2Δ0 met15Δ0 ura3Δ0; YFR051c::kanMX4; p415 CHI-12*	This study
15.	CHI 13	(*BY4743 Spore*) *MATa his3Δ1 leu2Δ0 met15Δ0 ura3Δ0; YFR051c::kanMX4; p415 CHI-13*	This study
16.	CHI 14	(*BY4743 Spore*) *MATa his3Δ1 leu2Δ0 met15Δ0 ura3Δ0; YFR051c::kanMX4; p415 CHI-14*	This study
17.	CHI 15	(*BY4743 Spore*) *MATa his3Δ1 leu2Δ0 met15Δ0 ura3Δ0; YFR051c::kanMX4; p415 CHI-15*	This study
18.	Ret2 I145A	(*BY4743 Spore*) *MATa his3Δ1 leu2Δ0 met15Δ0 ura3Δ0; YFR051c::kanMX4; p415 ret2 I145A*	This study
19.	Ret2 I148A	(*BY4743 Spore*) *MATa his3Δ1 leu2Δ0 met15Δ0 ura3Δ0; YFR051c::kanMX4; p415 ret2 I148A*	This study
20.	Ret2 I149A	(*BY4743 Spore*) *MATa his3Δ1 leu2Δ0 met15Δ0 ura3Δ0; YFR051c::kanMX4; p415 ret2 I149A*	This study
21.	Ret2 I155A	(*BY4743 Spore*) *MATa his3Δ1 leu2Δ0 met15Δ0 ura3Δ0; YFR051c::kanMX4; p415 ret2 I155A*	This study
22.	BY4741- TAP	*MATa his3Δ0 leu2Δ0 met15Δ0 ura3Δ0; sec27-TAP::URA3*	This study
23.	δc*-TAP	(*BY4743 Spore*) *MATa his3Δ1 leu2Δ0 met15Δ0 ura3Δ0; YFR051c::kanMX4; pRS303 Btδ*COP; *sec27-TAP::URA3*	This study
24.	Ret2LD2α-TAP	(*BY4743 Spore*) *MATa his3Δ1 leu2Δ0 met15Δ0 ura3Δ0; YFR051c::kanMX4; p415 ret2LD2α; sec27-TAP::URA3*	This study
25.	CHI-10-TAP	(*BY4743 Spore*) *MATa his3Δ1 leu2Δ0 met15Δ0 ura3Δ0; YFR051c::kanMX4; p415 CHI10; sec27-TAP::URA3*	This study
26.	Ret2LD-TAP	(*BY4743 Spore*) *MATa his3Δ1 leu2Δ0 met15Δ0 ura3Δ0; YFR051c::kanMX4; p415 ret2LD; sec27-TAP::URA3*	This study
27.	BY4741-Δ*sec28*	*MATa his3Δ0 leu2Δ0 met15Δ0 ura3Δ0; YIL076W::NatR*	This study
28.	Ret2-Δ*sec28*	(*BY4743 Spore*) *MATa his3Δ1 leu2Δ0 met15Δ0 ura3Δ0; YIL076W::NatR; YFR051c::kanMX4; p415 ret2*	This study
29.	Ret2LD2α-Δ*sec28*	(*BY4743 Spore*) *MATa his3Δ1 leu2Δ0 met15Δ0 ura3Δ0; YIL076W::NatR; YFR051c::kanMX4; p415 ret2LD2α*	This study
30.	Ret2LD2α Q146F	(*BY4743 Spore*) *MATa his3Δ1 leu2Δ0 met15Δ0 ura3Δ0; YFR051c::kanMX4; p415 ret2LD2α Q146F*	This study
31.	Ret2LD2α N152T	(*BY4743 Spore*) *MATa his3Δ1 leu2Δ0 met15Δ0 ura3Δ0; YFR051c::kanMX4; p415 ret2LD2α N152T*	This study
32.	Ret2LD2α K153Q	(*BY4743 Spore*) *MATa his3Δ1 leu2Δ0 met15Δ0 ura3Δ0; YFR051c::kanMX4; p415 ret2LD2α K153Q*	This study
33.	Ret2LD2α T158K	(*BY4743 Spore*) *MATa his3Δ1 leu2Δ0 met15Δ0 ura3Δ0; YFR051c::kanMX4; p415 ret2LD2α T158K*	This study

Table S2. Plasmids used in this study

No.	Plasmids	Addgene ID	Database ID	Source
1.	p415 CHI 1	73863	Z1280	This study
2.	p415 CHI 2	73864	Z1281	This study
3.	p415 CHI 3	73865	Z1283	This study
4.	p415 CHI 4	73866	Z1284	This study
5.	p415 CHI 5	73867	Z1285	This study
6.	p415 CHI 6	73868	Z1286	This study
7.	p415 CHI 7	73869	Z1287	This study
8.	p415 CHI 8	73870	Z1288	This study
9.	pRS303 Bt δCOP	73871	AE1540	This study
10.	p415 Ret2	73872	AE1541	This study
11.	p415 Ret2LD2α	73873	AE1518	This study
12.	p415 δCLD2α	73874	AE1519	This study
13.	p415 Ret2LD	73875	AE1520	This study
14.	p415 δCLD	73876	AE1521	This study
15.	p415 Ret2LD+δC2α	73877	AE1516	This study
16.	p415 δCLD+Ret2-2α	73878	AE1523	This study
17.	p415 CHI 9	73879	AF1551	This study
18.	p415 CHI 10	73880	AF1553	This study
19.	p415 CHI 12	73881	AF1557	This study
20.	p415 CHI 13	73882	AH1658	This study
21.	p415 CHI 14	73883	AH1660	This study
22.	p415 CHI 15	73884	AH1662	This study
23.	p415 Ret2 I145A	73885	AI1732	This study
24.	p415 Ret2 I148A	73886	AI1733	This study
25.	p415 Ret2 I149A	73887	AI1734	This study
26.	p415 Ret2 I155A	73888	AI1735	This study
27.	pGEX6P1- Mst7-Erp1CT	73920		This study
28.	pGEX6P1-GCN4cc-Erp1CT	73921		This study
29.	pGEX6P1- Mst7-Erp2CT	73922		This study
30.	pGEX6P1-GCN4cc-Erp2CT	73923		This study
31.	p415 Ret2LD2α Q146F	75259		This study
32.	p415 Ret2LD2α N152T	75260		This study
33.	p415 Ret2LD2α K153Q	75261		This study
34.	p415 Ret2LD2α T158K	75262		This study
35.	p416 PMP2-YFP-LRKRS	—	M650	14
36.	p416 PMP2-YFP-KKXX	—	N654	14
37.	p416 PMP2-YFP-NVRNRRK	—	R890	14
38.	p416 PMP2-YFP-KKK	—	M643	14
39.	p416 PMP2-YFP-AAXX	—	N655	14
40.	p416 PMP2-YFP-Task3C44T	—	S901	27
41.	pGEX6P1-MST27-LRKRS	—	F291	14
42.	pGEX6P1-MST27-KKXX	—	O732	14